Energy-Like Stability of Interconnected Grid-Forming Inverters with Potential-Sensitive Virtual Inertia

1st Yu Zhang
School of Artificial Intelligence and Automation
Huazhong University of Science and Technology
Wuhan, China
yuzhang_hust@hust.edu.cn

2nd Xiao-Kang Liu
School of Artificial Intelligence and Automation
Huazhong University of Science and Technology
Wuhan, China
xiaokangliu@hust.edu.cn

3th Feng Xiao
School of Control and Computer Engineering
North China Electric Power University
Beijing, China
fengxiao@ncepu.edu.cn

4rd Yan-Wu Wang
School of Artificial Intelligence and Automation
Huazhong University of Science and Technology
Wuhan, China
wangyw@hust.edu.cn

***Abstract*—This paper investigates the synchronization stability of interconnected grid-forming inverters governed by droop or virtual synchronous generator (VSG) control. A novel concept of potential-sensitive virtual inertia is introduced, in which each inverter's effective inertia varies adaptively with the network phase configuration. To analyze the resulting second-order Kuramoto-type dynamics, an energy-like Lyapunov function is constructed that generalizes the kinetic-potential energy structure. Rigorous analysis demonstrates that the proposed inertia design preserves asymptotic synchronization while ensuring bounded transient potential energy. Numerical studies validate that potential-sensitive inertia improves phase coherence and stability margins compared with conventional constant-inertia droop or VSG models.**

***Index Terms*—Grid-forming inverters, potential-sensitive inertia, energy-like Lyapunov function, synchronization stability.**

I. Introduction

With the rapid proliferation of renewable energy sources and distributed energy storage systems, modern power systems are increasingly characterized by reduced mechanical inertia and damping. This loss of natural inertia undermines system frequency stability and transient performance, prompting the development of virtual synchronous generator (VSG) and droop control strategies that emulate the electromechanical dynamics of traditional synchronous machines [1].

Early implementations of the VSG concept aimed to reproduce synchronous machine dynamics with fixed virtual inertia and damping. However, in [2], the stability margin of a VSG control deteriorates under strong-grid conditions, motivating the introduction of adaptive inertia control to maintain stability across varying grid strengths. Similar researches were made in [3] and [4], where adaptive and dual-adaptive inertia schemes were proposed to balance the trade-off between active power response and frequency regulation. These works revealed that constant virtual inertia cannot ensure optimal dynamic performance under changing operating conditions.

Building on this, advanced distributed and reinforcement learning-based control approaches have been explored. For instance, Saadatmand et al. [5] employed adaptive critic design for optimal inertia regulation in resistive-inductive microgrids. In [6], a distributed adaptive inertia method was developed to suppress power oscillations in multi-VSG systems. Recent contributions have extended adaptive inertia to hierarchical microgrid control and ancillary service provision. In [7], an adaptive inertia framework was combined with nonlinear voltage-frequency droops to support stable AC/DC microgrid operation. Similarly, Chang et al. [8] integrated adaptive inertia with a novel power-sharing mechanism to ensure both frequency support and equitable load distribution among parallel inverters. In [9], an adaptive inertia and damping were embedded to enhance frequency stability, demonstrating measurable improvements in frequency nadir and change rate. More recently, adaptive inertia concepts have been generalized to large-scale power grids in [10], where time-varying inertia was shown to outperform both fixed and electromechanical inertia in damping inter-area oscillations.

To further enhance adaptability and intelligence, machine learning and optimization-based approaches have emerged. Deep reinforcement learning was adopted in [11] to realize nonlinear inertia adaptation for grid-forming systems. In [12], a frequency-gradient based adaptive inertia controller was

This work is supported by the National Natural Science Foundation of China under Grant 62473164, the Key Research and Development Project of Hubei Province under Grant 2025BAB013, and the State Key Laboratory of Alternate Electrical Power System with Renewable Energy Soureces (Grant No. LAPS250008).

979-8-3315-8138-1

proposed to improve the transient frequency stability across diverse conditions.

Despite these advances, most adaptive inertia schemes remain heuristic or rely on empirical tuning based frequency of the linear system model, lacking a unified global theoretical foundation that accounts for the potential-sensitive inertia and its influence on system dynamics. Moreover, the physical consistency between adaptive inertia control and the underlying energy functions of power systems has not been systematically addressed. Motivated by these observations, this paper develops an energy-based modeling and analysis framework for interconnect grid-forming inverters with potential-sensitive inertia, enabling rigorous Lyapunov-based stability analysis and offering a physically consistent foundation for adaptive inertia design. The main contributions of this paper are given as follows.

1) A new inertia mechanism is proposed, where each inverter's effective virtual inertia adapts to the network phase configuration through a potential-dependent term. Different from frequency-based adaptive inertia control methods such as [9], [12], this design reflects the physical coupling among inverters and enhances the collective synchronization behavior.
2) An energy-like Lyapunov framework is developed that generalizes the conventional kinetic-potential energy structure to systems with potential-sensitive inertia. Compared with the system stability proven by linearization, such as [10], the asymptotic synchronization of the proposed system is rigorously given under mild damping conditions, ensuring that the constructed Lyapunov function remains non-increasing in the phase-cohesive region.

II. Preliminary

In renewable energy power systems, inverter-based distributed generators can be represented as second-order oscillators under suitable control strategies. We summarize the derivation for both droop-controlled inverters $i \in \mathcal{N}_d$ and VSG-controlled inverters $j \in \mathcal{N}_v$ with $\mathcal{N} = \mathcal{N}_d \cup \mathcal{N}_v$, and give the stability analysis of the resulting second-order Kuramoto model.

A. Second-Order Kuramoto Model for Interconnected Grid-Forming Inverters

The droop control law with filtered power measurement is $\omega_i = \omega_0 - k_{p,i}(\hat{P}_i - P_i^0), i \in \mathcal{N}_d$, where ω_i is the inverter frequency, ω_0 is the nominal frequency of the power system. $\hat{P}_i$ is the filtered active power, P_i^0 is the power setpoint, and $k_{p,i}$ is the droop gain. The power measurement is filtered by $\tau_i \dot{\hat{P}}_i + \hat{P}_i = P_i$ with τ_i being the filter time constant, where P_i is the output power of the inverter i. Taking the derivative of the frequency and substituting the filter dynamics leads to the following second-order swing-like dynamics [1].

$$m_i \ddot{\theta}_i + d_i \dot{\theta}_i = P_i^0 - P_i, \quad i \in \mathcal{N}_d, \tag{1}$$

where $m_i = \tau_i / k_{p,i}$, $d_i = 1/k_{p,i}$, and $\dot{\theta}_i = \omega_i - \omega_0$.

For the inverters operating under VSG control [13],

$$m_i \dot{\omega}_i + d_i(\omega_i - \omega_0) = P_i^0 - P_i, \quad i \in \mathcal{N}_v, \tag{2}$$

where m_i is the virtual inertia explicitly set in the controller, and d_i is the damping coefficient. Approximating the power grid with lossless lines yields $P_i \approx \sum_j K_{ij} \sin(\theta_i - \theta_j) + P_{L,i}$ with $K_{ij} = |V_i||V_j||B_{ij}|$. $|V_i|$ and $|V_j|$ are the voltage amplitude of the inverters i and j with B_{ij} being the transmission line susceptance. Then, the final second-order (inertial) Kuramoto model is given as follows [14].

$$m_i \ddot{\theta}_i + d_i \dot{\theta}_i = P_i^* - \sum_{j \in \mathcal{N}} K_{ij} \sin(\theta_i - \theta_j), \quad i \in \mathcal{N}, \tag{3}$$

where local net power injection is $P_i^* = P_i^0 - P_{L,i}$ with $P_{L,i}$ being the load active power.

From the above derivation, we have that both droop-controlled and VSG-controlled inverters reduce to a second-order heterogeneous-inertia Kuramoto model. The main difference is that droop-based inertia emerges from the power measurement filter, while VSG inertia is explicitly set. Heterogeneity arises from differences in m_i, d_i, and K_{ij} among inverters.

B. Energy-Based Stability for Constant Inertia

Consider the second-order heterogeneous-inertia Kuramoto model for inverter-based power system, we define the kinetic energy as $T = \frac{1}{2}\sum_i m_i \dot{\theta}_i^2$, and the potential energy as $U = \sum_i P_i^* \theta_i - \sum_{i<j} K_{ij} \cos(\theta_i - \theta_j)$. Then, the total energy function $E(\theta, \dot{\theta}_i) = T + U$ is

$$E(\theta, \dot{\theta}_i) = \frac{1}{2}\sum_i m_i \dot{\theta}_i^2 + \sum_i P_i^* \theta_i - \sum_{i<j} K_{ij} \cos(\theta_i - \theta_j), \tag{4}$$

which serves as a Lyapunov candidate for stability analysis. The kinetic energy T captures the frequency deviations of inverters, including their inertia property. The potential energy U depends on phase differences, reflecting network coupling and power flow balance. The time derivative of (4) along the system trajectories is

$$\begin{aligned} \dot{E} &= \sum_i m_i \dot{\theta}_i \ddot{\theta}_i + \sum_i \frac{\partial U}{\partial \theta_i} \dot{\theta}_i \\ &= \dot{\theta}_i \sum_i \Big(m_i \ddot{\theta}_i + P_i^* - \sum_j K_{ij} \sin(\theta_i - \theta_j) \Big). \end{aligned} \tag{5}$$

Based on the system dynamics (3), we can derive that $\dot{E} = -\sum_i d_i \dot{\theta}_i^2 \leq 0$, indicating that the total energy is non-increasing due to damping. Damping d_i ensures asymptotic convergence to equilibrium, providing energy dissipation and transient stability. The equilibrium θ_i^* satisfies $P_i^* = \sum_j K_{ij} \sin(\theta_i^* - \theta_j^*), i \in \mathcal{N}$, corresponding to a minimum of the potential energy.

C. Relationship Between the Hessian of the Potential Energy and System Stability

As the equilibrium θ^* of (3) satisfies $\nabla U(\theta^*) = 0$, and the Hessian $H(\theta^*) = \nabla^2 U(\theta^*)$ determines the local curvature of

979-8-3315-8138-1

the potential landscape, which is given as follows.

$$H(\theta^*) = B^T \operatorname{diag}\big(K_{ij}\cos(\theta_i^* - \theta_j^*)\big)\, B, \tag{6}$$

where $B \in \mathbb{R}^{|\mathcal{E}|\times|\mathcal{N}|}$ is the incidence matrix of the power system network and each diagonal entry of $\operatorname{diag}(\cdot)$ corresponds to a transmission line $(i,j) \in \mathcal{E}$.

According to the Hessian definition, 1) if the Hessian is positive definite, the equilibrium corresponds to a strict local minimum of the potential, implying that any small perturbation from P_i^0 and $P_{L,i}, i \in \mathcal{N}$ increases the energy E and induces restoring forces that drive the state back toward θ^*. 2) If the Hessian is positive semidefinite but not strictly positive, the potential landscape becomes flat in some directions, yielding marginal or weak stability. This phenomenon occurs near stability boundaries, such as when phase differences approach 90° in an inverter-based system. 3) If the Hessian is indefinite, the equilibrium is a saddle point of the potential energy. Perturbations in directions associated with negative eigenvalues reduce the potential energy and generate forces that push the system away from the equilibrium, leading to divergence, phase drift, or pole-slipping behavior.

Then, we have that the Hessian entries depend explicitly on the phase differences. Positive curvature (i.e., $\cos(\theta_i - \theta_j) > 0$) strengthens synchronizing forces, while negative curvature indicates loss of stability. The Hessian therefore directly encodes the phase-cohesiveness requirement, stability margin, and the admissible synchronization region in inverter-based systems. As a result, the definiteness properties of the Hessian provide a precise and physically interpretable criterion for assessing and guaranteeing local stability in interconnected grid-forming inverter-based systems.

III. Potential-Sensitive Inertia Design

To leverage this curvature information for stability enhancement, we introduce a potential-sensitive adaptive inertia that adjusts automatically with the phase-cohesiveness level. Since the Hessian curvature directly depends on $\cos(\theta_i - \theta_j)$, weakening as phase differences approach the stability boundary and becoming negative in unstable regions, the synchronizing stiffness decreases precisely when the risk of divergence increases. Thus, we design

$$m_i(\boldsymbol{\theta}) = m_{0i} \min_j \cos(\theta_i - \theta_j), \quad m_{0i} > 0, \tag{7}$$

where the inertia responds to real-time curvature degradation and enhances the frequency regulation flexibility with sufficient damping for reinforcing stability.

Note that the proposed potential-sensitive virtual inertia operates within the outer-loop dynamics (e.g., droop or VSG control) with relatively low bandwidth. The use of slow-varying phase angle measurements ensures that inertia adaptation is naturally bandwidth-limited, avoiding interactions with faster inner voltage and current control loops.

Assumption 1. *(*Phase cohesiveness*) The operating region satisfies $|\theta_i - \theta_j| < \frac{\pi}{2}$ for all $(i,j) \in \mathcal{E}$. Hence $\cos(\theta_i - \theta_j) > 0$ and $m_i(\boldsymbol{\theta}) > 0$.*

Assumption 2. *(*Bounded speeds*) There exists $v_{\max} > 0$ such that $\max_i |\dot{\theta}_i(t)| \le v_{\max}$ for all t.*

Theorem 1. *Consider the system (3) with the potential-sensitive inertia (7) under Assumptions 1-2. If the damping coefficients satisfy* (13)*, then all trajectories starting in the cohesive set converge to the equilibrium manifold defined by $P_i^* = \sum_{j\in\mathcal{N}} K_{ij}\sin(\theta_i^* - \theta_j^*)$ and $\dot{\theta}_i^* = 0, i \in \mathcal{N}$.*

Proof: Define the energy-like Lyapunov function

$$V(\boldsymbol{\theta}, \dot{\boldsymbol{\theta}}) = \tfrac{1}{2}\sum_{i\in\mathcal{N}} m_i(\boldsymbol{\theta})\dot{\theta}_i^2 + U(\boldsymbol{\theta}). \tag{8}$$

Under Assumption 1, V is positive definite with respect to the synchronized equilibrium. Differentiating (8) along solutions of (3) yields

$$\begin{aligned}\dot{V} &= \sum_{i\in\mathcal{N}} \Big(\tfrac{1}{2}\dot{m}_i\dot{\theta}_i^2 + m_i\dot{\theta}_i\ddot{\theta}_i\Big) + \sum_{i\in\mathcal{N}} \frac{\partial U}{\partial \theta_i}\dot{\theta}_i \\ &= \sum_{i\in\mathcal{N}} \Big(\tfrac{1}{2}\dot{m}_i\dot{\theta}_i^2 - d_i\dot{\theta}_i^2\Big).\end{aligned} \tag{9}$$

On any region where the minimizing index $j^\star(i) = \arg\min_j \cos(\theta_i - \theta_j)$ is unique, $m_i(\boldsymbol{\theta}) = m_{0i}\cos(\theta_i - \theta_{j^\star(i)})$. Then,

$$\dot{m}_i = -m_{0i}\sin(\theta_i - \theta_{j^\star(i)})(\dot{\theta}_i - \dot{\theta}_{j^\star(i)}). \tag{10}$$

Since $|\sin(\cdot)| \le 1$ and by Assumption 2, $|\dot{m}_i| \le m_{0i}|\dot{\theta}_i - \dot{\theta}_{j^\star(i)}| \le 2m_{0i}v_{\max}$. Then,

$$\Big|\tfrac{1}{2}\dot{m}_i\dot{\theta}_i^2\Big| \le m_{0i}v_{\max}\dot{\theta}_i^2. \tag{11}$$

Substituting (11) into (9),

$$\dot{V} \le -\sum_i (d_i - m_{0i}v_{\max})\,\dot{\theta}_i^2. \tag{12}$$

Therefore, if each node satisfies

$$d_i > m_{0i}v_{\max}, \tag{13}$$

then $\dot{V} \le -\gamma\sum_i \dot{\theta}_i^2$ with $\gamma = \min_i(d_i - m_{0i}v_{\max}) > 0$. ∎

Condition (13) requires that the local damping coefficient dominates the maximum effective rate of inertia variation induced by the potential-sensitive term $\cos(\theta_i - \theta_j)$. In practice, d_i is a freely tunable parameter in grid-forming inverter controllers, while $v_{\max}$ is bounded by grid safety requirements and inverter protection limits. Therefore, the condition can be satisfied through coordinated tuning of inertia and damping gains. Intuitively, as phase differences approach the stability boundary, the adaptive inertia reduces the kinetic energy stored in the system, which enhances the effectiveness of damping and ensures convergence of inverter phases to synchrony.

Assumption 2 bounds the phase velocities ($\max_i |\dot{\theta}_i(t)| \le v_{\max}$) to ensure the Lyapunov-based stability analysis is valid under normal operation. During large disturbances or faults, the potential-sensitive inertia together with damping still helps limit kinetic energy and promotes transient stabilization as the system returns to the cohesive operating region.

Note that the implementation of (7) requires neighboring

979-8-3315-8138-1

phase angle θ_j, which may be obtained via local sensing or communication. Due to the continuous damping effect of the controller, small delays or occasional missing measurements are generally tolerated.

Remark 1. *Different from ω or $\dot{\omega}$ based adaptive inertia control methods in [9], [12], the designed potential-sensitive inertia method (7) focuses on the system stability boundary and reflects the physical coupling among inverters and enhances the collective synchronization behavior. The enhancement of transient performances, including stability margin and phase cohesiveness, is tested in the following simulations.*

Remark 2. *An energy-like Lyapunov framework (8) is developed that generalizes the conventional kinetic-potential energy structure to systems with potential-sensitive inertia. Compared with the linearization methods in [10], the asymptotic synchronization of the proposed system is rigorously given under mild damping conditions (13).*

IV. Simulations

The simulation verification is conducted on a three-inverter power system to evaluate and compare the performance of constant and designed potential-sensitive inertia mechanisms (7). The system parameters are configured as follows. The base inertia constants are $\mathbf{M}_0 = [0.20,\ 0.25,\ 0.22]^{\mathrm{T}}$ pu·s^2, and damping coefficients are given by $\mathbf{D} = [0.30,\ 0.33,\ 0.30]^{\mathrm{T}}$ pu. The initial net power injection are defined as $\mathbf{P}^*_{\text{initial}} = [0.8,\ -0.4,\ -0.4]^{\mathrm{T}}$ pu. The coupling matrix is specified as $\mathbf{K} = \begin{bmatrix} 0 & 1.0 & 0.5 \\ 1.0 & 0 & 0.8 \\ 0.5 & 0.8 & 0 \end{bmatrix}$ pu. The nominal frequency of the power system is $f_0 = 60$ Hz, and the initial phase angles are initialized as $\boldsymbol{\theta}_{\text{init}} = [0.0,\ 0.3,\ -0.2]^{\mathrm{T}}$ radians. The simulations are conducted on a heterogeneous-inertia Kuramoto system mathematical model, which is rigorously derived from the full inverter dynamics. This model captures the essential synchronization and frequency regulation behaviors, providing insight into the practical impact of potential-sensitive inertia mechanisms.

A. Phase Cohersiveness Performance Test

To assess the system's phase dynamic response, a power disturbance is introduced at $t = 10$ s by altering the net power injection to $\mathbf{P}^* = [1.2,\ -1.5,\ 0.3]^{\mathrm{T}}$ pu.

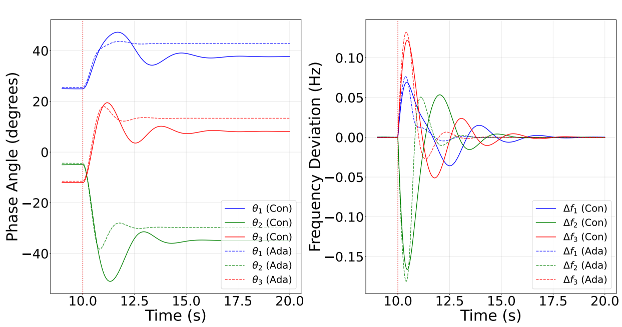

Fig. 1: (a) Phase angle, (b) Frequency deviation.

From Fig. 1, both the phase angle difference and frequency deviation converge to the same values for both constant and adaptive inertia cases. This indicates that the system equilibrium (steady-state operating point) is unchanged by the potential-sensitive inertia adaptation mechanism.

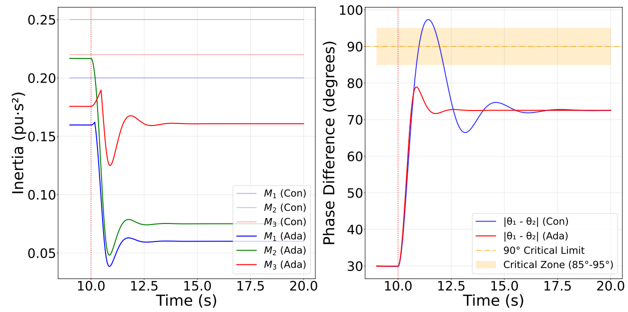

Fig. 2: (a) Adaptive inertia evolution, (b) Phase separation.

As shown in Fig. 2 (a), the maximum phase separation after disturbance is reduced from 97.34° (constant inertia) to 78.91° (adaptive inertia). From Fig. 2 (b), the constant inertia system spends 729 time steps in this risky region, while the adaptive inertia spends 0 time steps, with the time step being 0.01.

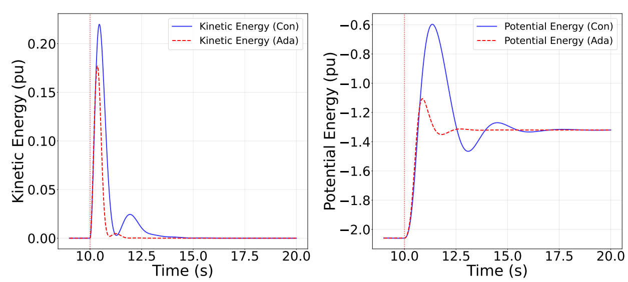

Fig. 3: (a) Kinetic energy, (b) Potential energy.

From Fig. 3, after a disturbance, the system with adaptive inertia exhibits a lower kinetic energy peak compared to the constant inertia case. Specifically, the maximum kinetic energy observed post-disturbance is reduced from approximately 0.22 pu (constant inertia) to 0.18 pu (adaptive inertia), representing a reduction of about 19%. This lower energy peak indicates that adaptive inertia helps absorb and dissipate the disturbance energy more effectively, thereby mitigating the risk of excessive oscillations and improving system stability. Furthermore, the adaptive inertia method provides a faster phase convergence rate. The phase angle differences between nodes return to their steady-state values more rapidly in the adaptive inertia system. Specifically, the time required for the phase difference to settle within 5% of its final value is reduced from 5.28 seconds (constant inertia) to 1.92 seconds (adaptive inertia), demonstrating a 63.6% improvement in convergence speed. This accelerated synchronization enhances the system's ability to maintain coherent operation and recover from large disturbances.

B. Stability Margin Performance Test

This case compares the stability margin of constant and adaptive inertia systems under a severe power imbalance

979-8-3315-8138-1

$\mathbf{P}^* = [1.28, -1.58, 0.3]^{\mathrm{T}}$ pu. This disturbance drives the constant inertia system beyond its stability limit, resulting in a complete loss of synchronism, while the adaptive inertia system maintains stable operation.

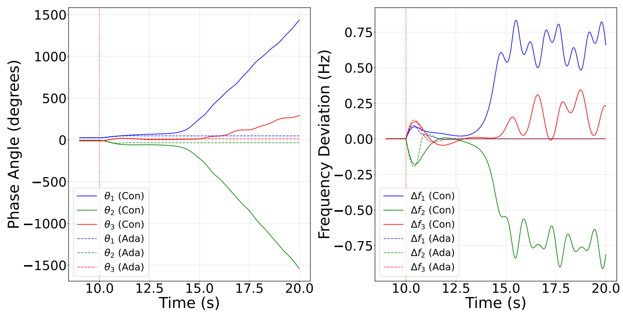

Fig. 4: (a) Phase angle, (b) Frequency deviation.

From Fig. 4, the maximum phase separation in the constant inertia case reaches $2976.8°$, corresponding to multiple pole slips, whereas the adaptive inertia confines it to only $84.3°$. The potential-sensitive system also eliminates all time spent in the critical $85°$-$95°$ separation zone, compared to 155 time steps for the constant inertia case.

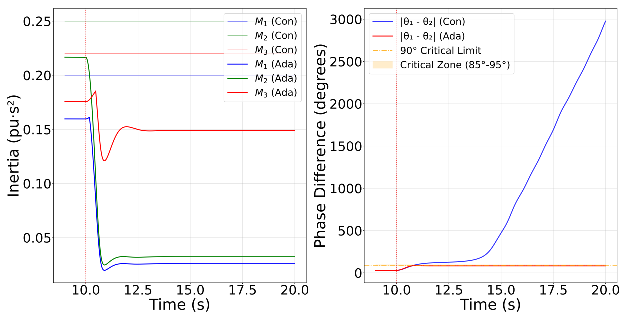

Fig. 5: (a) Adaptive inertia evolution, (b) Phase separation.

From Fig. 5, the adaptive inertia mechanism dynamically adjusts between 0.020 and 0.244 pu·s^2, achieving a $4.5\times$ variation range compared to the fixed inertia case. The negative correlation between phase difference and inertia demonstrates self-regulation, as inertia automatically decreases with phase separation, thereby enhancing the flexibility of frequency regulation.

From a system-level perspective, the adaptive inertia significantly enhances robustness and resilience. Physically, these results confirm that the adaptive mechanism redistributes inertia according to the system's instantaneous potential, decreasing inertia to enhance frequency regulation flexibility as phase deviations approach the stability boundary and thus preventing instability.

V. Conclusion

This paper has presented a potential-sensitive virtual inertia mechanism for enhancing the synchronization stability of interconnected grid-forming inverters. By allowing each inverter's effective inertia to vary with the network phase configuration, the proposed method captures the underlying potential curvature and strengthens collective synchronizing behavior. An energy-like Lyapunov function was constructed to generalize the kinetic-potential energy structure to systems with configuration-dependent inertia, and rigorous analysis established asymptotic synchronization under mild damping conditions. Simulation studies demonstrated that the proposed adaptive inertia improves transient performance compared with conventional constant-inertia droop or VSG models. From a practical perspective, the proposed approach relies on phase difference information among inverters, and addressing implementation challenges such as measurement synchronization, communication delays, and decentralized phase estimation constitutes an important direction for future work.

References

[1] J. Liu, Y. Miura, and T. Ise, "Comparison of dynamic characteristics between virtual synchronous generator and droop control in inverter-based distributed generators," *IEEE Transactions on Power Electronics*, vol. 31, no. 5, pp. 3600–3611, 2016.

[2] L. Huang, C. Yang, M. Song, H. Yuan, H. Xie, H. Xin, and Z. Wang, "An adaptive inertia control to improve stability of virtual synchronous machines under various power grid strength," in *2019 IEEE Power & Energy Society General Meeting (PESGM)*, 2019.

[3] X. Hou, Y. Sun, X. Zhang, J. Lu, P. Wang, and J. M. Guerrero, "Improvement of frequency regulation in VSG-based AC microgrid via adaptive virtual inertia," *IEEE Transactions on Power Electronics*, vol. 35, no. 2, pp. 1589–1602, 2020.

[4] M. Li, W. Huang, N. Tai, L. Yang, D. Duan, and Z. Ma, "A dual-adaptivity inertia control strategy for virtual synchronous generator," *IEEE Transactions on Power Systems*, vol. 35, no. 1, pp. 594–604, 2020.

[5] S. Saadatmand, P. Shamsi, and M. Ferdowsi, "Adaptive critic design-based reinforcement learning approach in controlling virtual inertia-based grid-connected inverters," *International Journal of Electrical Power & Energy Systems*, vol. 127, p. 106657, 2021.

[6] S. Fu, Y. Sun, Z. Liu, X. Hou, H. Han, and M. Su, "Power oscillation suppression in multi-VSG grid with adaptive virtual inertia," *International Journal of Electrical Power & Energy Systems*, vol. 135, p. 107472, 2022.

[7] F. Perez, G. Damm, C. M. Verrelli, and P. F. Ribeiro, "Adaptive virtual inertia control for stable microgrid operation including ancillary services support," *IEEE Transactions on Control Systems Technology*, vol. 31, no. 4, pp. 1552–1564, 2023.

[8] G. W. Chang and K. T. Nguyen, "A new adaptive inertia-based virtual synchronous generator with even inverter output power sharing in islanded microgrid," *IEEE Transactions on Industrial Electronics*, vol. 71, no. 9, pp. 10 693–10 703, 2024.

[9] W. Zhang, W. Wu, H. Wang, F. Blaabjerg, M. Orabi, and L. Yuan, "Virtual oscillator-controlled inverters with adaptive virtual inertia and damping to support frequency stability," in *IECON 2024 - 50th Annual Conference of the IEEE Industrial Electronics Society*, 2024.

[10] J. Fritzsch and P. Jacquod, "Stabilizing large-scale electric power grids with adaptive inertia," *PRX Energy*, vol. 3, p. 033003, 2024.

[11] D. Yang, S. Huang, C. Guo, Y. Zhou, P. Tan, L. Xiong, T. Lin, and W. Han, "Deep reinforcement learning-based adaptive inertia control for grid-forming power system," in *2025 4th International Conference on Smart Grid and Green Energy (ICSGGE)*, 2025, pp. 423–428.

[12] D. Rigato, D. Biadene, P. Magnone, and T. Caldognetto, "Adaptive inertia controller for grid-forming converters," *IFAC-PapersOnLine*, vol. 59, no. 9, pp. 327–332, 2025.

[13] X. Meng, J. Liu, and Z. Liu, "A generalized droop control for grid-supporting inverter based on comparison between traditional droop control and virtual synchronous generator control," *IEEE Transactions on Power Electronics*, vol. 34, no. 6, pp. 5416–5438, 2019.

[14] A. Sajadi, R. W. Kenyon, and B.-M. Hodge, "Synchronization in electric power networks with inherent heterogeneity up to 100% inverter-based renewable generation," *Nature communications*, vol. 13, no. 1, p. 2490, 2022.

979-8-3315-8138-1